*catalysts*

MDPI

*Article*

# Fast Microwave Synthesis of Gold-Doped $TiO_2$ Assisted by Modified Cyclodextrins for Photocatalytic Degradation of Dye and Hydrogen Production

**Cécile Machut [1,*], Nicolas Kania [1], Bastien Léger [1], Frédéric Wyrwalski [1], Sébastien Noël [1], Ahmed Addad [2], Eric Monflier [1] and Anne Ponchel [1]**

1 University Artois, CNRS, Centrale Lille, Univ. Lille, UMR 8181–UCCS–Unité de Catalyse et Chimie du Solide, F-62300 Lens, France; nicolas.kania@univ-artois.fr (N.K.); bastien.leger@univ-artois.fr (B.L.); frederic.wyrwalski@univ-artois.fr (F.W.); sebastien.noel@univ-artois.fr (S.N.); eric.monflier@univ-artois.fr (E.M.); anne.ponchel@univ-artois.fr (A.P.)

2 University Lille, CNRS, INRA, Centrale Lille, UMR 8207-UMET-Unité Matériaux et Transformations, F-59000 Lille, France; ahmed.addad@univ-lille.fr

* Correspondence: cecile.machut@univ-artois.fr

Received: 29 June 2020; Accepted: 16 July 2020; Published: 18 July 2020


**Abstract:** A convenient and fast microwave synthesis of gold-doped titanium dioxide materials was developed with the aid of commercially available and common cyclodextrin derivatives, acting both as reducing and stabilizing agents. Anatase titanium oxide was synthesized from titanium chloride by microwave heating without calcination. Then, the resulting titanium oxide was decorated by gold nanoparticles thanks to a microwave-assisted reduction of $HAuCl_4$ by cyclodextrin in alkaline conditions. The materials were fully characterized by UV-Vis spectroscopy, X-Ray Diffraction (XRD), Transmission Electron Microscopy (TEM), and $N_2$ adsorption-desorption measurements, while the metal content was determined by Inductively Coupled Plasma Optical Emission Spectroscopy (ICP-OES). The efficiency of the $TiO_2$@Au materials was evaluated with respect to two different photocatalytic reactions, such as dye degradation and hydrogen evolution from water.

**Keywords:** photocatalysis; photodegradation; nanoparticles; gold; $TiO_2$; cyclodextrins

## 1. Introduction

During the past decades, photocatalysis received extensive research interest for both limiting toxic wastes and developing clean and renewable sources of energy. Indeed, the association of a semiconductor with the sunlight in order to remove pollutants [1,2] or to produce hydrogen fuel by water splitting [3] could provide a sustainable solution to the crucial problems of environmental pollution and energy shortages [4].

Among a large number of photocatalysts, $TiO_2$ has been extensively investigated due to its good properties such as low cost, non-toxicity, and good stability [5,6]. Anatase phase is particularly recognized for its high photocatalytic efficiency. However, its large band gap (3.2 eV) combined with a high recombination rate of the photogenerated electron/hole pairs ($e^-/h^+$) reduce the photon-to-charge carriers conversion efficiency, but also limit the use in photochemical applications under visible or solar light.

In order to overcome these drawbacks and improve the photocatalytic performance of semiconductors, one of the promising strategies consists in introducing noble metals at the surface of $TiO_2$, such as gold nanoparticles [7]. Indeed, the combination with gold nanoparticles aims at inhibiting the electron-hole pair recombination by trapping electrons and facilitating the transfer of holes on the $TiO_2$ surface [8]. Gold nanoparticles (Au NPs) are also known to enhance the activity

of $TiO_2$ under visible-light irradiation due to the localized surface plasmon resonance of Au NPs in the visible light spectrum [9]. However, it is well accepted that the photocatalytic activity of such $TiO_2$@Au composites can strongly depend on the particle size of Au NPs [10] and optimal synthetic conditions must be found, especially to prevent the aggregation of gold nanoparticles [11,12].

Over the last decade, cyclodextrins and derivatives have received great interest in the field of synthesis and stabilization of metallic nanoparticles in aqueous medium [13]. These macrocyclic oligosaccharides, which are well-known to form inclusion complexes with numerous guest molecules via supramolecular interactions [14], can also be used as capping agents to stabilize zerovalent metal nanoparticles, such as Au NPs. Owing to the numerous hydroxyl groups attached to the CD rims, they can also act as efficient reducing agents for the synthesis of Au NPs [15–19]. However, to the best of our knowledge, the use of cyclodextrins to prepare $TiO_2$@Au composites through simple methods of synthesis has been scarcely investigated. Most synthetic routes involve the use of chemically modified cyclodextrins bearing thiol pendant groups as metal binding sites. Their preparations require multistep and complex synthetic procedure as well as the use of time-consuming purification methods. For instance, Zhu et al. developed a method to synthesize $TiO_2$ decorated by the assembly of per-6-thio-β-cyclodextrin and gold nanoparticles. The resulting composite showed very good efficiency for the degradation of methyl orange (MO) under UV light [20]. More recently, $TiO_2$ nanosheets consisting of the combination of Au nanoparticles and mono-6-thio-β-cyclodextrin were prepared for the electrochemical detection of trace of methyl parathion pesticide [21].

Recently, we have reported a sol-gel method using cyclodextrins as both structure-directing agents and metal-complexing agents to self-assemble titania and gold colloids in composite materials with controlled porosity and uniform metal dispersion [22]. Among the various cyclodextrins examined, the $TiO_2$@Au material prepared using the commonly used randomly methylated β-CD (RAME-β-CD) have shown, after calcination, the best catalytic performance for the photodegradation of organic pollutants in water under visible light, due to a good compromise between its textural properties, crystallinity, and Au particle size. However, the preparation of such plasmonic photocatalysts involved a multistep process that occurred over several days (including acid hydrolysis, peptization, maturation, drying, and finally calcination at a high temperature of 500 °C to form Au NPs).

In recent years, microwave (MW) irradiation techniques have received considerable attention in the field of nanomaterial synthesis by inducing or enhancing chemical reactions [23–25]. The use of microwave heating may offer several advantages over conventional heating, such as shorter reaction times, higher heating rates as well as higher uniformities of the products. In the literature, a few articles were already devoted to microwave-assisted synthesis of gold nanoparticles protected by cyclodextrin derivatives [16,26,27]. As a matter of fact, Aswathy et al. synthesized β-cyclodextrin capped Au NPs with a mean diameter of 20 nm within a few minutes [16]. More recently, Stiufiuc et al. used native cyclodextrins as reducing and capping agents during the microwave reduction of the gold precursor and obtained stable monodispersed gold nanospheres covered with either α-, β- or γ-CD [26]. However, to the best of our knowledge, the stabilization and anchorage of Au NPs on titania support thanks to CDs under microwave irradiation have never been explored.

In this context, we reported hereby a novel method for elaborating $TiO_2$@Au materials from a two-step microwave-assisted synthetic route without the need for high temperature calcination. Herein, the $TiO_2$ support is synthesized using a microwave-method by hydrolysis of titanium tetrachloride while the cyclodextrins are employed afterwards to produce size-controlled gold metallic nanoparticles anchored on the support, once again under microwave irradiation. We have focused our efforts on randomly methylated-β-CD (RAME-β-CD) and 2-hydroxypropyl-β-CD (HP-β-CD), which are both highly water-soluble and readily available commercially at relatively low cost. The impact of the nature of the carbohydrate precursor is investigated and discussed on the basis of different physicochemical characterizations, including X-ray diffraction (XRD), $N_2$ adsorption-desorption analysis, transmission electron microscopy (TEM), thermogravimetry analyses (TGA), and diffuse reflectance UV-Vis spectroscopy (DRUV-Vis). Finally, the efficiency of these photocatalysts is examined

with respect to two photocatalytic reactions carried out under near-UV-light irradiation (λ > 365 nm), i.e., the oxidative photodegradation of methyl orange and the hydrogen evolution reaction (HER).

## 2. Results and Discussion

As described in the Experimental Section, gold-doped $TiO_2$ materials have been synthesized at 150 °C with a fast microwave heating using cyclodextrins as reducing agent of the metal precursor and stabilizer of Au NPs. The synthetic procedure is schematically depicted in the Figure 1.

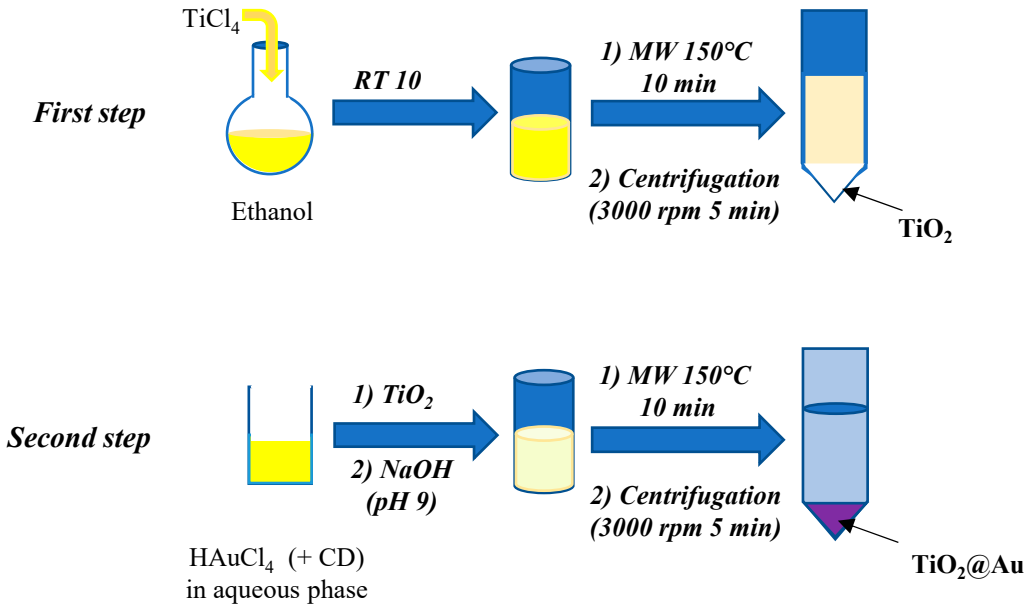


**Figure 1.** Schematic illustration of the two-step microwave (MW) procedure used for the $TiO_2$@Au materials synthesis.

Note that a bare $TiO_2$ control was also prepared in the same conditions as those described for the first step. These conditions were selected based on preliminary experiments, by varying the duration and power of the microwave irradiation, in order to optimize the crystallinity of our titania support. Indeed, the crystallinity is known to be a key factor in the photoactivity of $TiO_2$ particles. The XRD patterns of titania materials prepared from different heating programs (10, 30, and 45 min) and powers (320 and 600 W) are given for comparison in the Figure 2. With increasing the duration of heating at 320 W, we observe that the intensity of the XRD lines progressively increases and narrows, suggesting a growth in crystallite size. The planes (101), (004), (200), (105), and (211) associated to 2θ = 25.3°, 37.7°, 48°, and 55.2–55.9° respectively correspond to the anatase phase (Ti-A, JCPDS 21-1272). No XRD signals related to the presence of other crystalline phases such as rutile and brookite are detected. However, the most interesting effects are produced with the power of 600 W, which offers a very good compromise between crystallinity state and rate of anatase formation since this crystalline phase was obtained after only 10 min, this duration being considerably shorter than that applied for conventional sol-gel synthesis [28]. In line with this first optimization, the heating power of microwave irradiation was set to maximum (600 W) for all the further investigations, with a duration of temperature rise of 2 min from room temperature to 150 °C (isothermal step-time of 10 min).

The impact of the addition of gold by microwave-assisted reduction of the $TiO_2$ support was further investigated using mixtures of $HAuCl_4$ and modified cyclodextrins in alkaline conditions (see Figure 1, second step). We decided to use the randomly methylated β-cyclodextrin (RAME-β-CD) and the hydroxypropylated β-cyclodextrin (HP-β-CD) to stabilize Au NPs. Indeed, we particularly focused on these two CDs because of their high solubility in water and their beneficial effect on previously described gold-doped $TiO_2$ [22]. RAME-β-CD and HP-β-CD have also the advantages to

offer a number of available hydroxyl groups (8.4 per RAME-β-CD and 21 per HP-β-CD), which are known to play an important role in the reduction processes of metal cations [16,29].

The XRD patterns of these microwave-prepared titania@Au materials are reported in the Figure 3. For comparison, the XRD pattern of a control gold-doped $TiO_2$ prepared in ethanol (selected as model reducing agent), but without cyclodextrin, was also included ($TiO_2$@Au).

It can be noticed, that in addition to the reflections of anatase (Ti-A, JCPDS 21-1272), $TiO_2$@Au, $TiO_2$@Au-RB, and $TiO_2$@Au-HP present broad and low intense peaks at 2θ = 38.2°, 44.2°, 64.3°, and 78.1°, which could be respectively indexed to the (111), (200), (220), and (311) planes of gold with face-centered cubic crystalline structure phase (JCPDS 04-0784). The Au crystallite sizes could have been estimated from the line broadening of the (200) diffraction peak at 2θ = 44.2° by the Debye-Sherrer equation. Interestingly, for the control-doped $TiO_2$ material prepared using ethanol, the size of gold crystallites is ca. 15 nm, while it significantly decreases to ca. 8–10 nm for the materials prepared with HP-β-CD and RAME-β-CD.

The textural characteristics of the titania-based materials were then evaluated by $N_2$ adsorption-desorption analysis. All the samples exhibit type IV adsorption isotherms with distinct hysteresis loops appearing at P/P° ≈ 0.5–0.8, thus supporting the mesoporous character of the samples with a monomodal pore size of 4 nm (Figure S1 ESI and Table 1). The specific surface areas of the bare $TiO_2$ ($TiO_2$-control) is close to those prepared by gold-doped $TiO_2$ (240–260 $m^2.g^{-1}$). In the same way, the pore volumes and pore size values are substantially the same whether there is gold or not. The detailed surface properties and the gold loading determined by Inductively Coupled Plasma Optical Emission Spectroscopy (ICP-OES) measurements are summarized in the Table 1. ICP-OES analysis was used to quantitatively determine the gold content in our composites. Interestingly, the gold loading (≈2 wt %) corresponds to a gold incorporation efficiency around 80–90% of the initial amount of metal used during the synthesis.

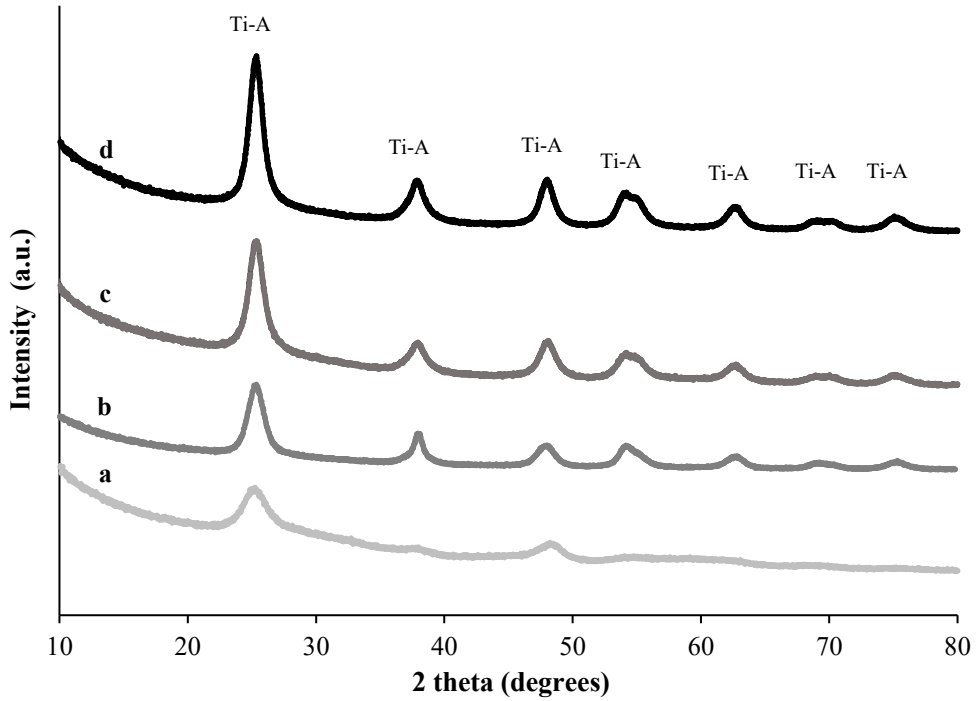


**Figure 2.** X-Ray Diffraction (XRD) patterns of titania-based materials prepared by microwave heating with different programs of heating (**a**) 320 W 3 min ramp then 10 min at 150 °C, (**b**) 320 W 3 min ramp then 30 min at 150 °C, (**c**) 320 W 3 min ramp then 45 min at 150 °C, and (**d**) 600 W 2 min ramp then 10 min at 150 °C.

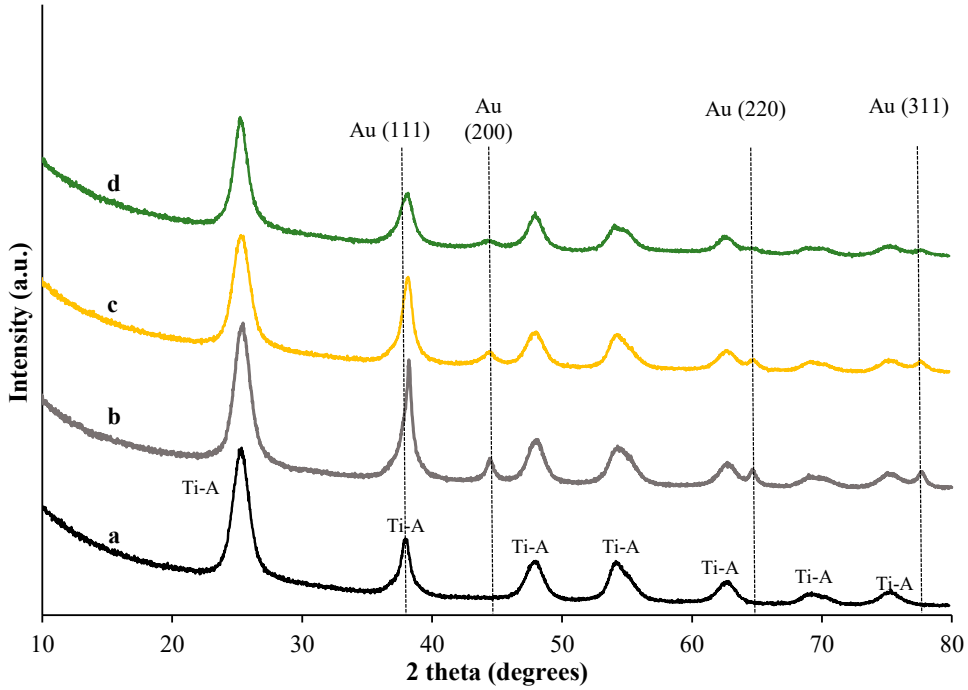


**Figure 3.** XRD patterns of titania materials prepared by microwave heating: (**a**) bare $TiO_2$, (**b**) $TiO_2$@Au prepared with ethanol, (**c**) $TiO_2$@Au-RB, and (**d**) $TiO_2$@Au-HP.

**Table 1.** Surface properties and gold loading of the different $TiO_2$ materials.

| Sample | $S_{BET}$ ($m^2.g^{-1}$) [a] | Pore Volume ($cm^3.\ g^{-1}$) [b] | Pore Size (nm) [c] | Au Content (wt %) [d] |
|---|---|---|---|---|
| $TiO_2$-control | 240 | 0.26 | 4.2 | - |
| $TiO_2$@Au | 230 | 0.30 | 4.8 | 2.3 |
| $TiO_2$@Au-RB | 230 | 0.22 | 4.0 | 2.0 |
| $TiO_2$@Au-HP | 260 | 0.30 | 4.8 | 2.2 |

[a] Specific surface area determined by the BET (Brunauer, Emmett et Teller) method in the relative pressure range of 0.1−0.25. [b] Pore volume computed by BJH. [c] Pore size determined by BJH. [d] Gold loading determined by ICP-OES analysis.

The morphology and structure of the $TiO_2$@Au materials were further characterized by TEM analyses (Figure 4). Whatever the materials, the presence of Au NPs deposited onto the surface of $TiO_2$ is observed. When the synthesis is performed under cyclodextrin-free conditions, with ethanol as reducing agent, TEM images (Figure 4a,b) show the presence of gold nanoparticles with a mean diameter of 13.5 nm but with a relatively broad size distribution ranging from 5 to 30 nm and a standard deviation of 5.3 nm (see histogram in Figure 4c). Note that larger gold nanoparticles with diameter ranging from 44 to 78 nm can be also observed (See Figure S2 in ESI).

Although a modest decrease in the mean particle size is noticed when modified β-cyclodextrins (12.5 nm for HP-β-CD and 12.9 nm for RAME-β-CD) are introduced during the microwave-assisted synthesis, it can be seen that, for these two catalysts, gold nanoparticles are more uniformly dispersed over the $TiO_2$ support. Narrower size distributions with standard deviations as low as 2.5–2.8 nm (see histograms in Figure 4f,j) can be clearly found, evidencing the stabilization of small and well-dispersed spherical Au NPs, as can be seen at high magnification (See Figure S3 in ESI). It provides an intimate contact between Au NPs and the $TiO_2$ mesoporous support. Conversely to what was observed with the ethanol procedure, no aggregation or formation of larger particles were observed over $TiO_2$@Au-HP and $TiO_2$@Au-RB.

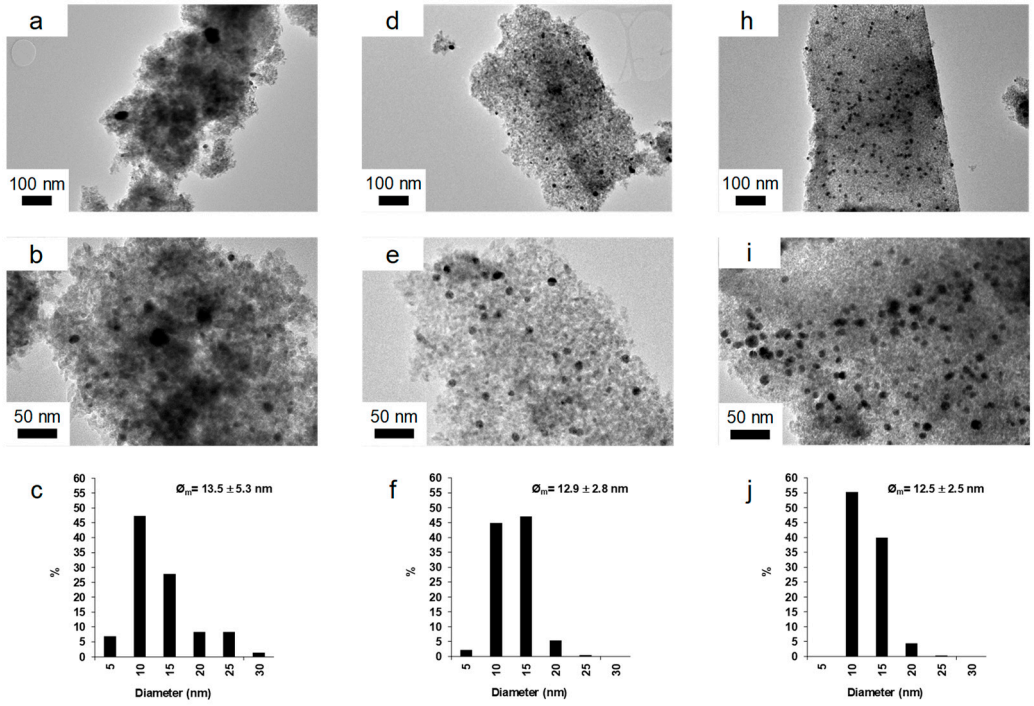


**Figure 4.** Transmission electron microscopy (TEM) images at magnification of ×25,000 (Scale bar = 100 nm) and ×62,000 (Scale bar = 50 nm) and size distribution of (**a**–**c**) $TiO_2$@Au, (**d**–**f**) $TiO_2$@Au-RB, (**h**–**j**) $TiO_2$@Au-HP.

As previously observed by several teams, cyclodextrins can stabilize metallic nanoparticles in aqueous solution [13]. Because of different types of interactions between the metal and the CDs (hydrophobic-hydrophobic interactions [30], non-covalent interactions between metal ions and hydroxyl groups of the CD [15]) the aggregation of gold nanoparticles can be avoided and it will result in a smaller particle size. As already observed with native CDs, RAME-β-CD and HP-β-CD are able to reduce $Au^{3+}$ thanks to their hydroxyl groups and then interact with the gold nanoparticles in order to prevent their agglomeration [31]. To the best of our knowledge, it is the first time that modified cyclodextrins are employed as both reducing agent of gold precursor and also stabilizing agent of gold nanoparticles.

Our materials were then characterized by UV-visible diffuse reflectance spectroscopy experiment. Figure 5 shows UV–Visible absorbance spectra and Tauc plots of $TiO_2$-control, $TiO_2$@Au, $TiO_2$@Au-RB and $TiO_2$@Au-HP materials. All the titania samples exhibit a broad absorption band around 330 nm corresponding to the charge transfer from O 2p valence band to Ti 3d conduction band [32]. Thus, the large band gap energy ($E_g$) of 3.20 eV estimated for the unmodified $TiO_2$ is in agreement with typical values reported in the literature for anatase structures. However, it is worth noting that, for the gold-doped $TiO_2$ samples prepared from cyclodextrins, a slight red-shift of the absorption edge of the $TiO_2$ semiconductor toward higher wavelengths was observed compared to pure $TiO_2$. The following sequence can be established in terms of $E_g$: $TiO_2$@Au-RB (2.70 eV) < $TiO_2$@Au-HP (2.95 eV) < $TiO_2$@Au (3.20 eV) = $TiO_2$ (3.20 eV).

As previously reported, the electrons can be transferred from the excited $TiO_2$ to the metallic nanoparticles and the electron accumulation increases the Fermi level of the nanoparticle to more negative potentials. Therefore, the involved edge energy in the electron transfer from $TiO_2$ to the metallic nanoparticles is lower than bare $TiO_2$ [33]. The lowest band gap values for the $TiO_2$@Au-RB and the $TiO_2$@Au-HP materials suggest that the contact between the two inorganic phases (gold and $TiO_2$) is enhanced when cyclodextrin is used during the Au NPs synthesis and this result is in good agreement with the TEM observations. However, the smallest value was found for the $TiO_2$@Au-RB so that we can suppose that the use of the RAME-β-CD promotes the most intimate contact between the

semiconductor and the metal. Further, another band is revealed at approximately 550 nm, confirming the presence of gold particles embedded in the $TiO_2$ matrix [34]. When neither cyclodextrin nor ethanol is added to the gold salt in the second step, no reduction of $Au^{3+}$ was noticed, the resulting powder remained white and its UV-Vis spectra was similar to that obtained for the bare $TiO_2$ (see Figure S4 in ESI).

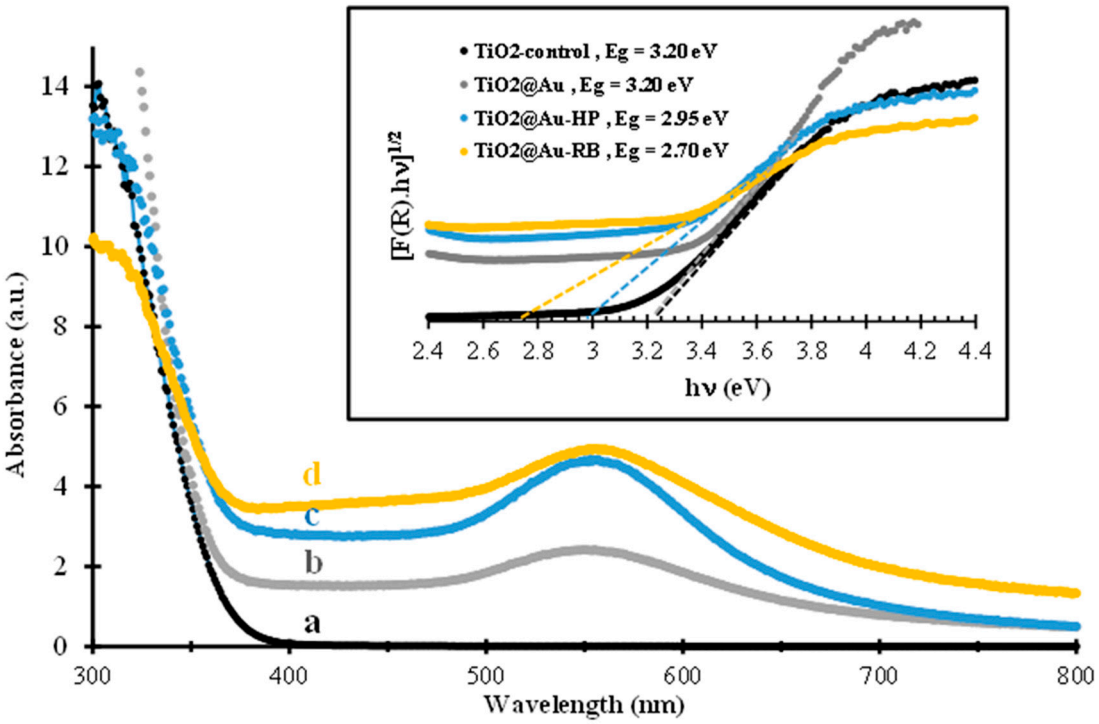


**Figure 5.** Diffuse Reflectance UV-Vis (DRUV-Vis) spectra of titania-based materials prepared by microwave heating: (**a**) bare $TiO_2$, (**b**) $TiO_2$@Au, (**c**) $TiO_2$@Au-HP, (**c**) and (**d**) $TiO_2$@Au-RB. In the inset, Tauc plots for the determination of the band gap values Tauc (indirect bad gap energy).

UV-Vis experiment and TEM images proved that modified CDs can act as both reducing agent of the metal precursor and capping agent of well-dispersed homogeneously dispersed Au NPs even in the presence of titanium dioxide. But to further characterize our materials and specially to know if cyclodextrins still remained in the $TiO_2$@Au-RB and the $TiO_2$@Au-HP samples, thermogravimetric analyses (TGA) were performed. The thermal profiles of $TiO_2$@Au, $TiO_2$@Au-RB, and $TiO_2$@Au-HP are shown in Figure 6.

The thermal patterns of the bare $TiO_2$ and the $TiO_2$@Au exhibit a one-step decomposition process with a weight loss in the 50–400 °C temperature range corresponding to the desorption of physically adsorbed water. The total weight loss for these samples are estimated to be 6.0 and 6.7 wt.%, respectively. The thermal profile of $TiO_2$@Au-RB exhibits a two-step decomposition process with a total weight loss of ca. 10.4 % at 1000 °C. The first weight loss (≈4%) in the 50–250 °C temperature range corresponds to the removal of physically adsorbed water, whereas the second weight loss (≈6%) in the 250–450 °C temperature range with a major weight loss at ca. 380 °C attributed to the thermal decomposition of the modified β-CD (Figure S5 in ESI). A similar profile was obtained with the $TiO_2$@Au-HP (Figure 6c) since this sample exhibited also a two-step decomposition process attributed to the removal of physically adsorbed water (≈6%) and to the thermal decomposition of residual HP-β-CD or its residues (≈11%) (see Figure S5 in ESI for the thermal profile of HP-β-CD alone). These thermal analyses proved that a small amount of saccharidic compounds (≈6 wt.% for the $TiO_2$@Au-RB and 11 wt.% for the $TiO_2$@Au-HP) remains adsorbed on our composite materials prepared with modified CDs even after the washing cycles. This result could be explained by the ability of CD derivatives to interact both with the gold nanoparticles and with the titania support. As previously described, we can suppose that after the

microwave reduction, cyclodextrin derivatives could be linked to the gold nanoparticles through weak interactions and covered the outer surface of the Au NPs [16,26]. In addition, cyclodextrins are known to be able to interact with the titanium dioxide through hydrogen bounds [35,36]. In fact, the hydroxyl groups located at the exterior of the torus favored the interactions of the cyclic oligosaccharides with the surface OH groups of titania. This latter hypothesis could also explain why the amount of organic compounds is higher in the $TiO_2$@Au-HP than in the $TiO_2$@Au-RB composite: the quantity of saccharidic compounds adsorbed on titania increases with the number of hydroxyl groups of the CD [37]. Because of a higher number of hydroxyl groups (21 vs. 8.4), the HP-β-CD is more adsorbed on the titania support than the RAME-β-CD. This hypothesis could also explain the larger $E_g$ observed for the $TiO_2$@Au-HP compared to the $TiO_2$@Au-RB composite: the residual organic compounds may reduce the contact between the Au NPs and the titanium dioxide [38].

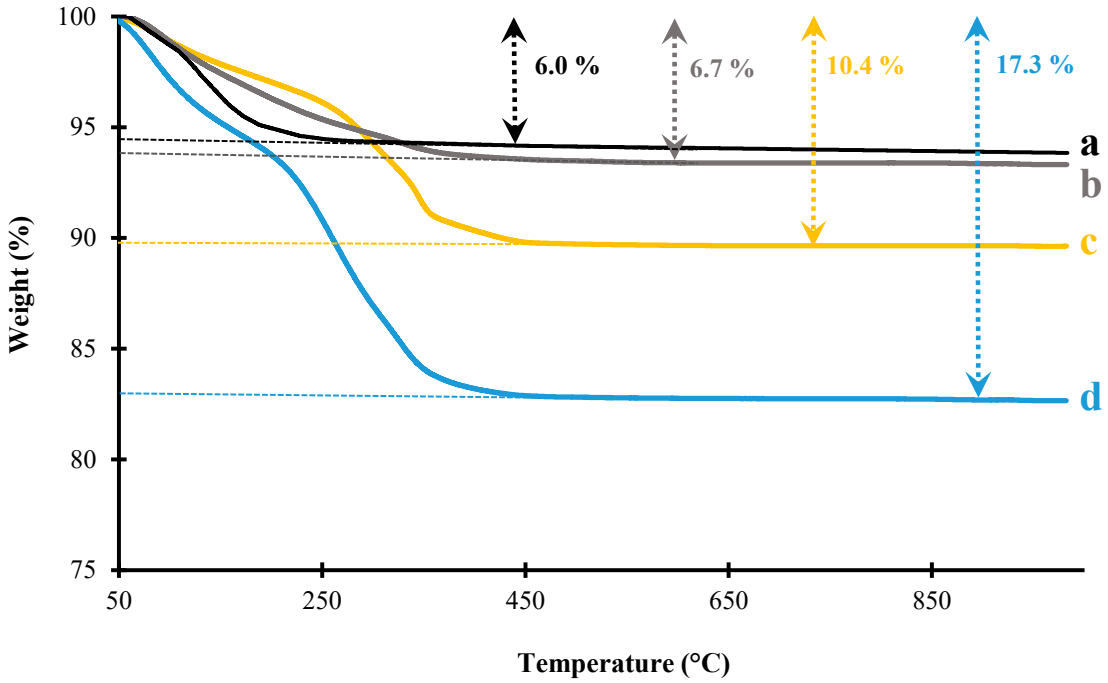


**Figure 6.** Thermogravimetric profiles for (**a**) bare $TiO_2$, (**b**) $TiO_2$@Au, (**c**) $TiO_2$@Au-RB, and (**d**) $TiO_2$@Au-HP.

According to the textural and structural studies, our titania-based materials exhibited interesting characteristics for photocatalytic applications. Indeed, the catalytic efficiency is known to be linked to two major physical properties: crystallinity and surface area of the photocatalysts [39].

With this microwave synthesis, only the anatase crystalline phase was obtained at low temperature (150 °C) without any additional calcination (or another thermal treatment) and this phase is known for its good activity in photocatalysis. On the other hand, good textural properties in terms of specific surface area, pore size, and pore volume could facilitate adsorption and diffusion of the target molecules onto the surface of the catalyst [40].

To confirm these hypotheses, the photocatalytic performances of the microwave gold-doped $TiO_2$ materials have been investigated through two different experiments. The redox properties of these materials have been firstly evaluated in the photodegradation of methyl orange (MO) in water. Briefly, an aqueous solution of MO (50 ppm) in the presence of the semi-conductors was irradiated at 365 nm and the concentration of the residual dye was regularly quantified by HPLC measurements. Prior to the photocatalytic study, the photostability of the organic dye was checked in a preliminary test without photocatalyst (Figure S6), and it was found that the concentration of MO remained unchanged during

the 1h test period. The performances of $TiO_2$@Au-RB and $TiO_2$@Au-HP are reported in the Figure 7. For comparison, $TiO_2$@Au prepared with ethanol was also tested (Figure 7a).

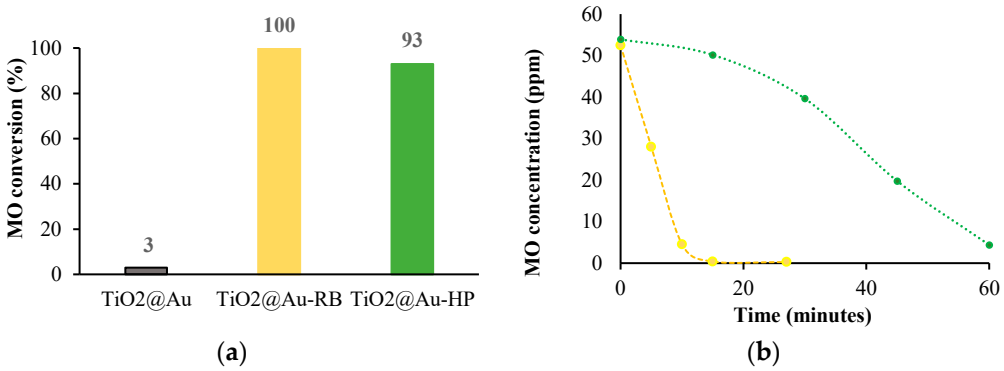


**Figure 7.** Photocatalytic performances of the gold-doped titania materials prepared by microwave heating for the degradation of methyl orange in near UV (λ = 365 nm): (**a**) Conversion of methyl orange after 60 min of irradiation (**b**) Evolution of the methyl orange concentration during one hour of irradiation for $TiO_2$@Au-RB (yellow) and $TiO_2$@Au-HP (green).

After 60 min under near UV irradiation, the dye was hardly degraded in the presence of the $TiO_2$@Au prepared without CD by microwave heating and this result is similar to thus obtained with bare $TiO_2$ (Figure S6). In contrast, after one hour of irradiation, the MO concentration was close to zero for the tests realized with the gold-doped $TiO_2$ prepared with modified cyclodextrins ($TiO_2$@Au-RB and $TiO_2$@Au-HP). The addition of modified CD during the synthesis of Au NPs in the presence of $TiO_2$ improved drastically the performances of the photocatalyst and this result is probably linked to the good dispersion of nanosized gold nanoparticles obtained from CDs over the support. In fact, small and well-dispersed metal islands deposited on the $TiO_2$ core are known to provide a favorable geometry for facilitating the interfacial charge transfer under UV irradiation [41]: the electrons of the titanium oxide are excited from the valence band to the conduction band and then migrate to Au clusters, which prevent the direct recombination of electrons and holes. For the $TiO_2$@Au-RB and $TiO_2$@Au-HP samples, we can suppose that the small and spherical Au NPs observed on the surface of the semi-conductor by TEM experiments act as electron sink to favor the oxidation and the reduction reactions. Conversely, large particles of metal are often harmful to the photocatalytic activity so that the $TiO_2$@Au prepared with ethanol as reducing agent was less efficient in our conditions [42]. Logically, large nanoparticles mobilize more gold atoms than small ones. With an equal metal loading, materials doped with large Au NPs offer fewer electronic reservoirs than those with small particles.

Additionally, the Figure 7b showed that the decrease of the MO amount was significantly faster in the presence of the microwave-assisted gold-doped $TiO_2$ prepared with RAME-β-CD compared to that prepared with HP-β-CD (Figure 7b). The lowest efficiency of the $TiO_2$@Au-HP compared to the $TiO_2$@Au-RB might be correlated to the highest band gap (as evidenced by DRUV-Vis experiment) and also to the amount of CDs residues in the final material (as evidenced by thermogravimetric analysis). In fact, we can suppose that the residual organic compounds decrease the contact between the semi-conductor and the gold and so reduce the electron transfer. Furthermore, the CDs residues could maybe mask some of the active sites of the semi-conductor or reduce the potential adsorption of the MO [43].

The recyclability and reuse of the most efficient photocatalyst ($TiO_2$@Au-RB) was also evaluated in the degradation of the MO. From Figure S7, it can be seen that the photocatalytic activity is stable during at least 3 runs. This study clearly showed the robustness of the catalyst and the strong embedment of the Au NPs onto the $TiO_2$ support.

Finally, we studied the behavior of the gold-doped $TiO_2$ in the production of hydrogen by photoreduction of water. Aqueous suspensions of the $TiO_2$@Au, $TiO_2$@Au-HP, and $TiO_2$@Au-RB were

irradiated at 365 nm in the presence of ethanol as the sacrificial agent. The result of the amount of hydrogen produced by photoreduction of water is reported in the Figure 8a.

When the $TiO_2$@Au-HP and the $TiO_2$@Au-RB were irradiated in water, hydrogen was quickly detected and the amount of $H_2$ was quantified as about 160 and 300 $\mu mol.h^{-1}.g^{-1}$ of catalyst, respectively. Compared to other $TiO_2$ catalysts in the literature [2,44], these amounts of produced hydrogen are promising since the power of our lamp is very low in comparison to Xe lamp usually used in such photocatalytic experiments. Moreover, the yield of hydrogen produced with our gold-doped catalyst was very high in comparison with that obtained with commercial anatase $TiO_2$ ($<2$ $\mu mol.h^{-1}.g^{-1}$) or with $TiO_2$@Au prepared with ethanol as reducing agent in the same conditions (about 3 $\mu mol.h^{-1}.g^{-1}$). As observed with the first photocatalytic test, the $TiO_2$@Au-RB was also more efficient than the$TiO_2$@Au-HP to produce hydrogen from water, probably due to the same reasons discussed above (i.e., twice as many organic compounds on the surface of the photocatalyst for the $TiO_2$@Au-HP than for the $TiO_2$@Au-RB). Finally, the amount of hydrogen produced is reproducible after several cycles of illumination (see for example Figure 8b with $TiO_2$@Au-RB) and stable during more than 10 h (ESI, Figure S8). This catalytic result proved that the introduction of small and uniform gold nanoparticles thanks to CDs reduction leads to a real boost of the photocatalytic performances of titanium dioxide even under UV irradiation and clearly confirmed the need of intimate contact with $TiO_2$ and Au to enhance the electron transfer between them.

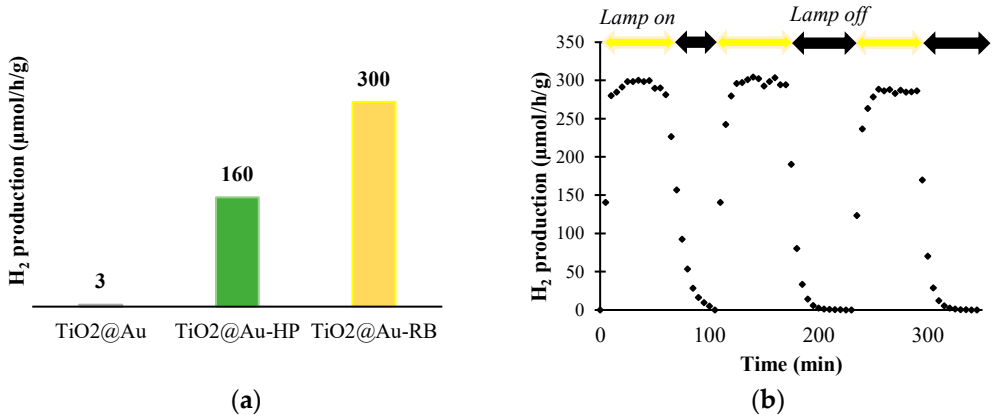


**Figure 8.** (**a**) Amount of hydrogen produced by photoreduction of water in the presence of gold-doped $TiO_2$ prepared by microwave heating process (100 mg of photocatalyst, 80 mL water, 20 mL ethanol, $\lambda = 365$ nm) (**b**) Evolution of the hydrogen production by photoreduction of water in the presence of $TiO_2$@Au-RB during 3 cycles of illumination.

## 3. Materials and Methods

### *3.1. Chemicals*

Randomly methylated β-cyclodextrin (RAME-β-CD) with an average degree of substitution of 1.8 methyl groups per glucopyranose unit (MW 1310 $g.mol^{-1}$) was a gift from Wacker Chemie GmbH (Lyon, France). Hydroxypropyl-β-cyclodextrin (HP-β-CD) with an average substitution of 0.6 $CH_2CH(OH)$-$CH_3$ groups per glucopyranose unit (MW 1380 $g.mol^{-1}$) was purchased from Roquette (Lestrem, France). Ethanol, methyl orange (MO) and $TiCl_4$ were purchased from Sigma-Aldrich (Quentin-Fallavier, France) while $HAuCl_4$ (49 wt.%) was provided by Strem Chemicals (Bischheim, France). All these reagents were used without purification.

### *3.2. Preparation of the Au/$TiO_2$ Materials with Cyclodextrins*

In a typical preparation, $TiO_2$ was prepared from $TiCl_4$ by microwave heating (CEM Mars instrument, Power 600 W) inspired by a method previously described by Wang et al. [45]. $TiCl_4$ (0.9 mL, 8.21 mmol) was quickly added to ethanol (25 mL) and stirred at room temperature during 10 min. Then,

the yellow solution was introduced in a Teflon microwave reactor equipped with temperature and pressure probes and heated to 150 °C during 10 min. The white suspension was centrifuged at 3000 rpm during 5 min. The supernatant was evacuated and the resulting white powder of $TiO_2$ was added to 20 mL of an aqueous solution of $HAuCl_4$ ($3.73 \times 10^{-5}$ mmol) and cyclodextrin ($4.04 \times 10^{-4}$ mmol). Note that this CD/Au molar ratio of about 10 has been chosen to promote the synthesis of spherical gold nanoparticles, in line with a previous work reported in the literature [46]. NaOH (0.5 M) was slowly added to the solid suspension in order to adjust the pH value at about 9. Then the mixture was transferred in a Teflon microwave reactor and was finally heated under microwave irradiation with the same program used to prepare $TiO_2$ from $TiCl_4$ (600 W, 150 °C, 10 min). To promote the synthesis of gold nanoparticles. At the end of the heating microwave program, the suspension was centrifuged and the purple powder was thoroughly washed with water before overnight drying at 100 °C. The gold-doped $TiO_2$ materials synthesized by microwave heating from RAME-β-CD and HP-β-CD were named as $TiO_2$@Au-RB and $TiO_2$@Au-HP, respectively. Additionally, note that a control gold-doped $TiO_2$ (denoted as $TiO_2$@Au) was also prepared in a very similar manner as the above described procedure, by substituting cyclodextrin for ethanol during the reduction process. The syntheses and characterizations have been reproduced several times.

### *3.3. Characterization Methods*

#### 3.3.1. Powder X-ray Diffraction

Powder X-ray diffraction data were collected on a Siemens D5000 X-ray diffractometer (Bruker, Palaiseau, France) in a Bragg-Brentano configuration with a Cu Kα radiation source. Scans were run over the angular domains $10° < 2\theta < 80°$ with a step size of 0.02° and a counting time of 2 s/step. Crystalline phases were identified by comparing the experimental diffraction patterns to Joint Committee on Powder Diffraction Standards (JCPDS) files for anatase. The treatment of the diffractograms was performed using the FullProf software [47] and its graphical interface WinPlotr [48]. The average crystallite size D was calculated from the Scherrer formula, $D = K\lambda/(\beta \cos \theta)$, where K is the shape factor (a value of 0.9 was used in this study, considering that the particles are spherical), λ is the X-ray radiation wavelength (1.54056 Å for Cu K), β is the full width at half-maximum (fwhm), and θ is the Bragg angle.

#### 3.3.2. Nitrogen Adsorption-Desorption Isotherms

Nitrogen adsorption-desorption isotherms were collected at −196 °C using an adsorption analyzer Micromeritics Tristar 3020 (Merignac, France). Prior to analysis, 200–400 mg samples were outgassed at 100 °C overnight to remove the species adsorbed on the surface. From $N_2$ sorption isotherms, specific surface areas were calculated by the BET method while pore size distributions were determined using the BJH model assuming a cylindrical pore structure. The relative errors were estimated to be the following: $S_{BET}$, 5%; pore volume (pv) (BJH), 5%; pore size (ps) (BJH), 20%.

#### 3.3.3. Diffuse Reflectance UV-Visible

Diffuse reflectance UV-visible spectra were collected using a Shimadzu UV-Vis NIR spectrometer (Marne-la-Vallée, France). $BaSO_4$ was used as the reference. Tauc plot analysis was performed for the calculation of the band gap energy (Eg). In fact, the Eg can be estimated by plotting $(F(R)\ h\nu)^n$ vs. hν and extrapolated from linear part of the curve to the hν x-axis intercept. To determine values of these forbidden energies, the absorption data were fitted to the Tauc relation for indirect band-gap transitions ($n = \frac{1}{2}$) [49].

#### 3.3.4. Thermogravimetric Analysis (TGA) Coupled with Differential Scanning Calorimetry (DSC)

Thermogravimetric Analysis (TGA) coupled with Differential Scanning Calorimetry (DSC) analyses were performed using a Mettler Toledo TGA/DSC3+ STARe system unit (Viroflay, France).

The samples were placed in aluminum oxide crucibles of 70 µL and heated from 40 to 1000 °C at 10 °C.min$^{-1}$ under a 50 mL.min$^{-1}$ air flow.

#### 3.3.5. ICP Optical Emission Spectrometry

ICP optical emission spectrometry was performed on an iCAP 7000 Thermo Scientific spectrometer (Les Ulis, France). For the quantification of gold loading, 10 mg of the Au/$TiO_2$ materials were introduced in 20 mL of aqua regia and then heated to 130 °C during one hour. Then the remaining $TiO_2$ was removed using a 0.2 µm pore filter. The resulting solution is finally diluted with pure water up to a final volume of 100 mL. The amount of gold incorporated in the material was determined using an external calibration with a gold ICP standard solution.

#### 3.3.6. Transmission Electron Microscopy (TEM)

Transmission Electron Microscopy (TEM) bright field observations were performed on a Tecnai G2 microscope (FEI, Hillsboro, Oregon, USA) operating at an accelerating voltage of 200 kV. The Au/$TiO_2$ powder was deposited directly on a carbon coated copper grid. Metal particle size distributions have been determined from the measurement of about 200 Au NPs. The nanoparticles were found in arbitrarily chosen area of the images using the program ImageJ software.

### *3.4. Photocatalytic Experiments*

#### 3.4.1. Photodegradation of Methyl Orange

The photocatalytic efficiency of the titania-based materials was first evaluated in the photodegradation of methyl orange (MO) carried out using quartz reactors of 5 mL. In a typical experiment, 10 mg of photocatalyst was added to 4 mL of a solution of methyl orange (50 ppm). After 30 min in the dark, UV irradiation was performed using a led UV light lamp (Opsytec λ = 365 nm, beam size = 0.785 cm$^2$, power of 0.2 W.cm$^{-2}$). Aliquots were centrifuged at regular intervals and the MO concentration in the supernatant was determined by high-performance chromatography (HPLC, PerkinElmer, Villebon-sur-Yvette, France) analyses using a PerkinElmer Pecosphere C18 (83 mm length × 4.6 mm diameter) column. An aqueous mixture of acetonitrile (20% (*v*/*v*)) was used as the mobile phase at a flow rate of 1 mL.min$^{-1}$. Aliquots of 50 µL of the sample was injected and analyzed using a photodiode array detector. The MO conversion given in percentage refers to the difference in the MO concentration before irradiation ($C_0$) and after 1 h of irradiation (C) divided by the MO concentration before irradiation (i.e., $100 \times (C_0 - C)/C_0$).

#### 3.4.2. Production of Hydrogen by Photoreduction of Water

Photocatalytic measurements for $H_2$ generation were carried out in a cylindrical pyrex reactor equipped with a quartz window by irradiating the titania-based materials in a 20 vol% ethanol-water solution (ethanol was used as hole-scavenger). As light source, we used the same LED UV light as that employed for the photocatalytic degradation of MO experiments described above in Section 3.4.1. The reactor operated at room temperature and atmospheric pressure and was kept under stirring at a constant speed of 1250 rpm. In a typical experiment, 100 mg of photocatalyst was added to a 100 mL of ethanol-water solution in the reactor. The catalytic solid suspension was then flushed with argon gas (420 mL.h$^{-1}$) for 60 min prior to photocatalysis. The amount of $H_2$ produced was measured on-line using a micro gas chromatograph (Micro-GC Agilent 490, Les Ulis, France) equipped with a thermal conductivity detector and two separating columns (Microsieve 10 m (5 Å) and 8 m-Paraplot U) operating with backflush injection (Ar as carrier gas).

## 4. Conclusions

In this work, an easy and fast preparation of Au loaded $TiO_2$ without calcination step is described. The addition of common modified cyclodextrin (methylated or hydroxypropylated) during the

microwave reduction of a gold precursor in the presence of $TiO_2$ led to an efficient photocatalyst both for pollutant photodegradation and photoreduction of water under near UV irradiation. The saccharidic macrocycle was responsible for a good stabilization of gold nanoparticles in aqueous solution so that these latter could not aggregate during the microwave synthesis and were deposited uniformly on the $TiO_2$ surface. Because of its lowest number of hydroxyl groups, the RAME-β-CD seems to be less adsorbed onto the surface of the final composite after the gold reduction and represents the most promising photocatalyst. It could be now interesting to study the photocatalytic performances of our materials under solar simulated lamp. However, this new and fast synthetic approach offers promising perspectives for photocatalytic depollution process and green energy production.

**Supplementary Materials:** The following are available online at http://www.mdpi.com/2073-4344/10/7/801/s1, Figure S1. N2 adsorption desorption isotherms of TiO2-control (a) gold decorated titania materials prepared without CD (TiO2@Au) (b) gold decorated titania materials prepared with HP-β-CD (TiO2@Au-HP) (c) gold decorated titania materials prepared with RAME-β-CD (TiO2@Au-RB) (d), Figure S2. TEM images of TiO2@Au catalyst at magnification of ×62,000, Figure S3. TEM images of (a) TiO2@Au-RBand (b) TiO2@Au-HB at magnification of ×490,000, Figure S4. UV-vis spectra of titania materials prepared by a two-step microwave heating procedure with HAuCl4 in a second step but without CD and without ethanol, Figure S5. TGA profiles for the RAME-β-CD and the HP-β-CD, Figure S6. Evolution of methyl orange concentration under irradiation (λ = 365 nm) as a function of time in the absence (open circle) or presence of the bare TiO2 prepared by microwave process (filled circle). Reaction conditions: TiO2, m = 10 mg; methyl orange solution, V = 4 mL (50 ppm) Figure S7. Performance of TiO2@Au-RB in three consecutive tests with reuse of the catalyst. Reaction conditions: 4 mL of a solution of methylorange (50 ppm), 10 mg of TiO2@Au-RB (λ = 365 nm, t = 10 min), Figure S8. Production of hydrogen by photoreduction of water (80 mL) in the presence of TiO2@Au-RB (100 mg) and ethanol (20 mL) as sacrificial agent (λ = 365 nm).

**Author Contributions:** Synthesis, catalytic tests, ICP, and UV experiments, C.M.; $N_2$ adsorption-desorption measurements and IR spectroscopy, N.K.; TEM analysis, B.L. and A.A.; XRD, A.P. and F.W.; catalysis, S.N.; supervision and reviewing results, reviewing the manuscript, English writing, C.M., E.M., and A.P. All authors have read and agreed to the published version of the manuscript.

**Funding:** This research received no external funding.

**Acknowledgments:** The TEM facility in Lille (France) is supported by the Conseil Régional du Nord Pas de Calais and the European Regional Development Fund (ERF). Chevreul Institute (FR 2638), Ministère de l'Enseignement Supérieur, de la Recherche et de l'Innovation, Région Hauts-de-France and FEDER are acknowledged for supporting and funding partially this work. The authors are grateful to the University of Artois for supporting this research through the Quality Research Bonus (Micro-GC Agilent 490 in 2018).

**Conflicts of Interest:** The authors declare no conflict of interest.

## References

1. Youa, J.; Guoa, Y.; Guob, R.; Liub, X. A review of visible light-active photocatalysts for water disinfection: Features and prospects. *Chem. Eng. J.* **2019**, *373*, 624–641. [CrossRef]
2. Boyjoo, Y.; Sun, H.; Liu, J.; Pareek, V.K.; Wang, S. A review on photocatalysis for air treatment: From catalyst development to reactor design. *Chem. Eng. J.* **2017**, *310*, 537–559. [CrossRef]
3. Jafari, T.; Moharreri, E.; Amin, A.S.; Miao, R.; Song, W.; Suib, S.L. Photocatalytic Water Splitting—The Untamed Dream: A Review of Recent Advances. *Molecules* **2016**, *21*, 900–929. [CrossRef]
4. Daghrir, R.; Drogui, P.; Robert, D. Modified $TiO_2$ for Environmental Photocatalytic Applications: A Review. *Ind. Eng. Chem. Res.* **2013**, *52*, 3581–3599. [CrossRef]
5. Chen, X.; Mao, S.S. Titanium Dioxide Nanomaterials: Synthesis, Properties, Modifications and Applications. *Chem. Rev.* **2007**, *107*, 2891–2959. [CrossRef]
6. Haider, A.J.; Jameel, Z.N.; Al-Hussaini, I.H. Review on: Titanium Dioxide Applications. *Energy Procedia* **2019**, *157*, 17–29. [CrossRef]
7. Khaki, M.R.D.; Shafeeyan, M.S.; Raman, A.A.A.; Daud, W.M.A.W. Application of doped photocatalysts for organic pollutant degradation—A review. *J. Environ. Manag.* **2017**, *198*, 78–94. [CrossRef] [PubMed]
8. Truppi, A.; Petronella, F.; Placido, T.; Margiotta, V.; Lasorella, G.; Giotta, L.; Giannini, C.; Sibillano, T.; Murgolo, S.; Mascolo, G.; et al. Gram-scale synthesis of UV–vis light active plasmonic photocatalytic nanocomposite based on $TiO_2$/Au nanorods for degradation of pollutants in water. *Appl. Catal. B Environ.* **2019**, *243*, 604–613. [CrossRef]

9. Cheng, L.; Zhang, D.; Liao, Y.; Li, F.; Zhang, H.; Xiang, Q. Constructing functionalized plasmonic gold/titanium dioxide nanosheets with small gold nanoparticles for efficient photocatalytic hydrogen evolution. *J. Colloid Interface Sci.* **2019**, *555*, 94–103. [CrossRef] [PubMed]
10. Iliev, V.; Tomova, D.; Bilyarska, L.; Tyuliev, G. Influence of the size of gold nanoparticles deposited on $TiO_2$ upon the photocatalytic destruction of oxalic acid. *J. Mol. Catal. A Chem.* **2007**, *263*, 32–38. [CrossRef]
11. Zhou, H.; Zheng, L.; Jia, H. Facile control of the self-assembly of gold nanoparticles by changing the capping agent structures. *Colloids Surf. A Physicochem. Eng. Asp.* **2014**, *450*, 9–14. [CrossRef]
12. Zielińska-Jurek, A.; Kowalska, E.; Sobczak, J.W.; Lisowski, W.; Ohtani, B.; Zaleska, A. Preparation and characterization of monometallic (Au) and bimetallic (Ag/Au) modified-titania photocatalysts activated by visible light. *Appl. Catal. B Environ.* **2011**, *101*, 504–514. [CrossRef]
13. Noël, S.; Léger, B.; Ponchel, A.; Philippot, K.; Denicourt-Nowicki, A.; Roucoux, A.; Monflier, E. Cyclodextrin-based systems for the stabilization of metallic(0) nanoparticles and their versatile applications in catalysis. *Catal. Today* **2014**, *235*, 20–32. [CrossRef]
14. Connors, K.A. The Stability of Cyclodextrin Complexes in Solution. *Chem. Rev.* **1997**, *97*, 1325–1358. [CrossRef] [PubMed]
15. Bhoi, V.I.; Kumar, S.; Murthy, C.N. Cyclodextrin encapsulated monometallic and inverted core–shell bimetallic nanoparticles as efficient free radical scavengers. *New J. Chem.* **2016**, *40*, 1396–1402. [CrossRef]
16. Aswathy, B.; Avadhani, G.S.; Suji, S.; Sony, G. Synthesis of β-cyclodextrin functionalized gold nanoparticles for the selective detection of $Pb^{2+}$ ions from aqueous solution. *Front. Mater. Sci.* **2012**, *6*, 168–175. [CrossRef]
17. Woo Chung, J.; Guo, Y.; Kwak, S.-Y.; Priestley, R.D. Understanding and controlling gold nanoparticle formation from a robust self-assembled cyclodextrin solid template. *J. Mater. Chem.* **2012**, *22*, 6017–6026. [CrossRef]
18. Huang, T.; Meng, F.; Qi, L. Facile Synthesis and One-Dimensional Assembly of Cyclodextrin-Capped Gold Nanoparticles and Their Applications in Catalysis and Surface-Enhanced Raman Scattering. *J. Phys. Chem. C* **2009**, *113*, 13636–13642. [CrossRef]
19. Pande, S.; Ghosh, S.K.; Praharaj, S.; Panigrahi, S.; Basu, S.; Jana, S.; Pal, A.I.; Tsukuda, T.; Pal, T. Synthesis of Normal and Inverted Gold-Silver Core-Shell Architectures in α-Cyclodextrin and Their Applications in SERS. *J. Phys. Chem. C* **2007**, *111*, 10806–10813. [CrossRef]
20. Zhu, H.; Goswami, N.; Yao, Q.; Chen, T.; Liu, Y.; Xu, Q.; Chen, D.; Lu, J.; Xie, J. Cyclodextrin–gold nanocluster decorated $TiO_2$ enhances photocatalytic decomposition of organic pollutants. *J. Mater. Chem. A* **2018**, *6*, 1102–1108. [CrossRef]
21. Fu, X.-C.; Zhang, C.; Li, X.-H.; Zhang, J.; Wei, G. Mono-6-thio-β-cyclodextrin-functionalized AuNP/two-dimensional $TiO_2$ nanosheet nanocomposite for the electrochemical determination of trace methyl parathion in water. *Anal. Methods* **2019**, *11*, 4751–4760. [CrossRef]
22. Lannoy, A.; Bleta, R.; Machut-Binkowski, C.; Addad, A.; Monflier, E.; Ponchel, A. Cyclodextrin-Directed Synthesis of Gold-Modified $TiO_2$ Materials and Evaluation of Their Photocatalytic Activity in the Removal of a Pesticide from Water: Effect of Porosity and Particle Size. *ACS Sustain. Chem. Eng.* **2017**, *5*, 3623–3630. [CrossRef]
23. Wen, P.; Wu, Z.; Han, Y.; Cravotto, G.; Wang, J.; Ye, B.-C. Microwave-Assisted Synthesis of a Novel Biochar-Based Slow-Release Nitrogen Fertilizer with Enhanced Water-Retention Capacity. *ACS Sustain. Chem. Eng.* **2017**, *5*, 7374–7382. [CrossRef]
24. Martina, K.; Baricco, F.; Berlier, G.; Caporaso, M.; Cravotto, G. Efficient Green Protocols for Preparation of Highly Functionalized β-Cyclodextrin-Grafted Silica. *ACS Sustain. Chem. Eng.* **2014**, *2*, 2595–2603. [CrossRef]
25. Tabasso, S.; Calcio Gaudino, E.; Acciardo, E.; Manzoli, M.; Bonelli, B.; Cravotto, G. Microwave-Assisted Protocol for Green Functionalization of Thiophenes With a Pd/b-Cyclodextrin Cross-Linked Nanocatalyst. *Front. Chem.* **2020**, *8*, 253. [CrossRef]
26. Stiufiuc, G.; Toma, V.; Moldovan, I.; Stiufiuc, R.; Lucaciu, C.M. One pot microwave assisted synthesis of cyclodextrins capped spherical gold nanoparticles. *Dig. J. Nanomater. Biostruct.* **2017**, *12*, 1089–1095.
27. Tsuji, M. Microwave-Assisted Synthesis of Metallic Nanomaterials in Liquid Phase. *ChemistrySelect* **2017**, *2*, 805–819. [CrossRef]

28. Qi, K.; Xin, J.H. Room-Temperature Synthesis of Single-Phase Anatase $TiO_2$ by Aging and its Self-Cleaning Properties. *ACS Appl. Mater. Interfaces* **2010**, *2*, 3479–3485. [CrossRef]
29. Pestovsky, Y.S.; Martínez-Antonio, A. Synthesis of Gold Nanoparticles by Tetrachloroaurate Reduction with Cyclodextrins. *Quim. Nova* **2018**, *41*, 926–932.
30. Liu, Y.; Male, K.B.; Bouvrette, P.; Luong, J.H.T. Control of the Size and Distribution of Gold Nanoparticles by Unmodified Cyclodextrins. *Chem. Mater.* **2003**, *15*, 4172–4180. [CrossRef]
31. Zhao, Y.; Huang, Y.; Zhu, H.; Zhu, Q.; Xia, Y. Three-in-One: Sensing; Self-Assembly and Cascade Catalysis of Cyclodextrin Modified Gold Nanoparticles. *J. Am. Chem. Soc.* **2016**, *138*, 16645–16654. [CrossRef] [PubMed]
32. Morawa Eblagon, K.; Pastrana-Martínez, L.M.; Pereira MF, R.; Figueiredo, J.L. Cascade conversion of cellobiose to gluconic acid: The large impact of the small modification of electronic interaction on the performance of Au/$TiO_2$ bifunctional catalysts. *Energy Technol.* **2018**, *6*, 1675–1686. [CrossRef]
33. Oros-Ruiza, S.; Zanellaa, R.; Prado, B. Photocatalytic degradation of trimethoprim by metallic nanoparticles supported on $TiO_2$-P25. *J. Hazard. Mater.* **2013**, *263*, 28–35. [CrossRef] [PubMed]
34. Wang, X.; Mitchell, D.R.G.; Prince, K.; Atanacio, A.J.; Caruso, R.A. Gold nanoparticle incorporation into porous titania networks using agarose gel templating technique for photocatlytic applications. *Chem. Mater.* **2008**, *20*, 3917–3926. [CrossRef]
35. Willner, I.; Eichen, Y.; Willner, B. Supramolecular semiconductor receptor assemblies: Improved electron transfer at $TiO_2$-β-cyclodextrin colloid interfaces. *Res. Chem. Intermed.* **1994**, *20*, 681–700. [CrossRef]
36. Zhang, X.; Wu, F.; Wang, Z.; Guo, Y.; Deng, N. Photocatalytic degradation of 4;4′-biphenol in $TiO_2$ suspension in the presence of cyclodextrins: A trinity integrated mechanism. *J. Mol. Catal. A Chem.* **2009**, *301*, 134–139. [CrossRef]
37. Lannoy, A.; Kania, N.; Bleta, R.; Fourmentin, S.; Machut-Binkowski, C.; Monflier, E.; Ponchel, A. Photocatalysis of Volatile Organic Compounds in water: Towards a deeper understanding of the role of cyclodextrins in the photodegradation of toluene over titanium dioxide. *J. Colloid Interface Sci.* **2016**, *461*, 317–325. [CrossRef]
38. May-Masnou, A.; Soler, L.; Torras, M.; Salles, P.; Llorca, J.; Roig, A. Fast and Simple Microwave Synthesis of $TiO_2$/Au Nanoparticles for Gas-Phase Photocatalytic Hydrogen Generation. *Front. Chem.* **2018**, *10*, 110. [CrossRef]
39. Kanna, M.; Wognawa, S. Mixed amorphous and nanocrystalline $TiO_2$ powders prepared by sol-gel method: Characterization and photocatalytic study. *Mater. Chem. Phys.* **2008**, *110*, 166–175. [CrossRef]
40. Wang, X.; Caruso, R.A. Enhancing photocatalytic activity of titania materials by using porous structures and the addition of gold nanoparticles. *J. Mater. Chem.* **2011**, *21*, 20–28. [CrossRef]
41. Dawson, A.; Kamat, P.V. Semiconductor-Metal Nanocomposites. Photoinduced Fusion and Photocatalysis of Gold-Capped $TiO_2$ ($TiO_2$/Gold) Nanoparticles. *J. Phys. Chem. B* **2001**, *105*, 960–966. [CrossRef]
42. Gołąbiewska, A.; Malankowska, A.; Jarek, M.; Lisowski, W.; Nowaczyk, G.; Jurga, S.; Zaleska-Medynska, A. The effect of gold shape and size on the properties and visible light-induced photoactivity of Au-$TiO_2$. *Appl. Catal. B Environ.* **2016**, *196*, 27–40. [CrossRef]
43. Luna, A.L.; Matter, F.; Schreck, M.; Wohlwend, J.; Tervoort, E.; Colbeau-Justin, C.; Niederberger, M. Monolithic metal-containing $TiO_2$ aerogels assembled from crystalline pre-formed nanoparticles as efficient photocatalysts for $H_2$ generation. *Appl. Catal. B Environ.* **2020**, *267*, 118660. [CrossRef]
44. Wang, B.; Shen, S.; Mao, S.S. Black $TiO_2$ for solar hydrogen conversion. *J. Mater.* **2017**, *3*, 96–111.
45. Wang, X.; Tian, J.; Fei, C.; Lv, L.; Wang, Y.; Cao, G. Rapid construction of $TiO_2$ aggregates using microwave assisted synthesis and its application for dye-sensitized solar cells. *RSC Adv.* **2015**, *5*, 8622–8629. [CrossRef]
46. Huang, Y.; Li, D.; Li, J. β-Cyclodextrin controlled assembling nanostructures from gold nanoparticles to gold nanowires. *Chem. Phys. Lett.* **2004**, *389*, 14–18. [CrossRef]
47. Rodriguez-Carvajal, J. FULLPROF: A Program for Rietveld Refinement and Pattern Matching Analysis. In *Abstracts of the Satellite Meeting on Powder Diffraction of the XV Congress of the IUCR, Toulouse, France*; International Union of Crystallography: Chester, UK, 1990; p. 127.

48. Roisnel, T.; Rodriguez-Carvajal, J. WinPLOTR: A Windows Tool for Powder Diffraction Pattern Analysis. In *Materials Science Forum, Proceedings of the 7th European Powder Diffraction Conference (EPDIC 7), Barcelona, Spain, 20–23 May 2000*; Delhez, R., Mittenmeijer, E.J., Eds.; Trans Tech Publications: Zurich, Switzerland, 2000; pp. 118–123.
49. Khore, S.K.; Kadam, S.R.; Naik, S.D.; Kale, B.B.; Sonawane, R.S. Solar light active plasmonic Au@$TiO_2$ nanocomposite with superior photocatalytic performance for $H_2$ production and pollutant degradation. *New J. Chem.* **2018**, *42*, 10958–10968. [CrossRef]